We are IntechOpen,
the world's leading publisher of
Open Access books
Built by scientists, for scientists

6,900
Open access books available

185,000
International authors and editors

200M
Downloads

Our authors are among the

154
Countries delivered to

TOP 1%
most cited scientists

12.2%
Contributors from top 500 universities

CLARIVATE ANALYTICS

BOOK CITATION INDEX

INDEXED

WEB OF SCIENCE™

Selection of our books indexed in the Book Citation Index
in Web of Science™ Core Collection (BKCI)

Interested in publishing with us?
Contact book.department@intechopen.com

Numbers displayed above are based on latest data collected.
For more information visit www.intechopen.com

Phenomenological Modelling of Cyclic Plasticity

Radim Halama[1], Josef Sedlák and Michal Šofer[1]
[1]Centre of Excellence IT4Innovations
Department of Mechanics of Materials
VŠB-Technical University of Ostrava
Czech Republic

1. Introduction

The stress-strain behaviour of metals under a cyclic loading is very miscellaneous and needs an individual approach for different metallic materials. There are many different models that have been developed for the case of cyclic plasticity. This chapter will address only so called phenomenological models, which are based purely on the observed behaviour of materials. The second section of this chapter describes the main experimental observations of cyclic plasticity for metals. Material models development for the correct description of particular phenomenon of cyclic plasticity is complicated by such effects as cyclic hardening/softening and cyclic creep (also called ratcheting). Effect of cyclic hardening/softening corresponds to hardening or softening of material response, more accurately to decreasing/increasing resistance to deformation of material subjected to cyclic loading. Some materials show very strong cyclic softening/hardening (stainless steels, copper, etc.), others less pronounced (medium carbon steels). The material can show cyclic hardening/softening behaviour during force controlled or strain controlled loading. On the contrary, the cyclic creep phenomenon can arise only under force controlled loading. The cyclic creep can be defined as accumulation of any plastic strain component with increasing number of cycles and can influence the fatigue life of mechanical parts due to the exhaustion of plastic ability of material earlier than the initiation of fatigue crack caused by low-cycle fatigue is started.

The third section of this chapter deals with the cyclic plasticity models included in the most popular Finite Element packages (Ansys, Abaqus, MSC.Nastran/Marc). A particular attention is paid to the calibration of classical nonlinear kinematic hardening models. Stress-strain behaviour of materials may be significantly different for proportional and non proportional loading, i.e. loading which leads to the rotation of principal stresses. In case of stainless steels an additional hardening occurs under non proportional loading. This additional hardening is investigated mostly under tension/torsion loading using the circular, elliptical, cross, star and other loading path shapes. Classical cyclic plasticity models implemented in the commercial Finite Element software are not able to describe well the non proportional hardening and correct prediction of multiaxial ratcheting is also problematic. This problem can be solved by implementation of more complex cyclic plasticity model to a FE code. As a conclusion there are briefly summarized phenomenological modelling theories of ratcheting. The main attention is focused on the most progressive group of cyclic plasticity models with a one yield surface only. The

AbdelKarim-Ohno model is also described, which gives very good prediction of ratcheting under uniaxial as well as multiaxial loading.

Comparison of the AbdelKarim-Ohno model and classical models is presented through simulations in the fourth section. Numerical analyses were performed for various uniaxial and multiaxial loading cases of specimen made from the R7T wheel steel. It is shown that classical models can also get sufficient ratcheting prediction when are correctly calibrated.

2. Experimental facts

Good understanding the nature of particular effects of cyclic plasticity plays a key role in the phenomenological modelling. Main findings from this chapter will be useful for a reader in the field of understanding the calibration of cyclic plasticity models and for correct numerical analysis results evaluation.

2.1 Bauschinger's effect

Bauschinger's effect is a basic and well known phenomenon of cyclic plasticity. It describes the fact that due to uniaxial loading of a specimen above yield limit in one direction the limit of elasticity in the opposite direction is reduced. As an example can serve the stress-strain curve corresponding to the first cycle of strain controlled low cycle fatigue test of the steel ST52 (see Fig.1). If the yield limit is marked as σ_Y, then the material during unloading from maximal axial stress state σ_1 behaves elastically up to the point, where the difference between maximal and immediate stress $\sigma_1 - \sigma_2$ is equal to the double of yield limit $2\sigma_Y$.
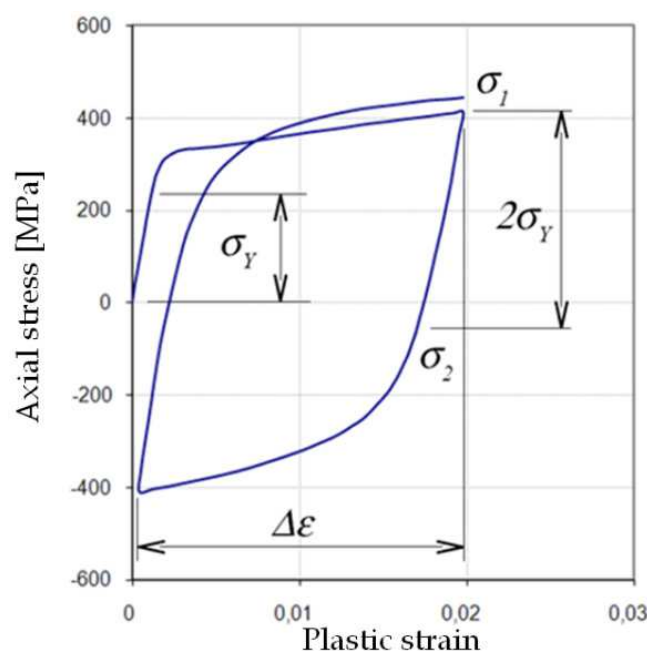

Fig. 1. Presentation of Bauschinger's effect.

2.2 Cyclic hardening/softening

Results of the micro structural changes in the beginning stage of cyclic loading are changes of physical properties and stress response in the material. Cyclic softening/hardening effect

relates to softening/hardening of material response or decreasing/increasing of resistance against material deformation under cyclic loading. Its intensity usually decrease with number of cycles until the saturated state is reached. During uniaxial cyclic loading, the condition is characterized by closed hysteresis loop. Transient responses in initial cycles caused by cyclic hardening/softening under plastic strain control and stress control are shown at the Fig.2.
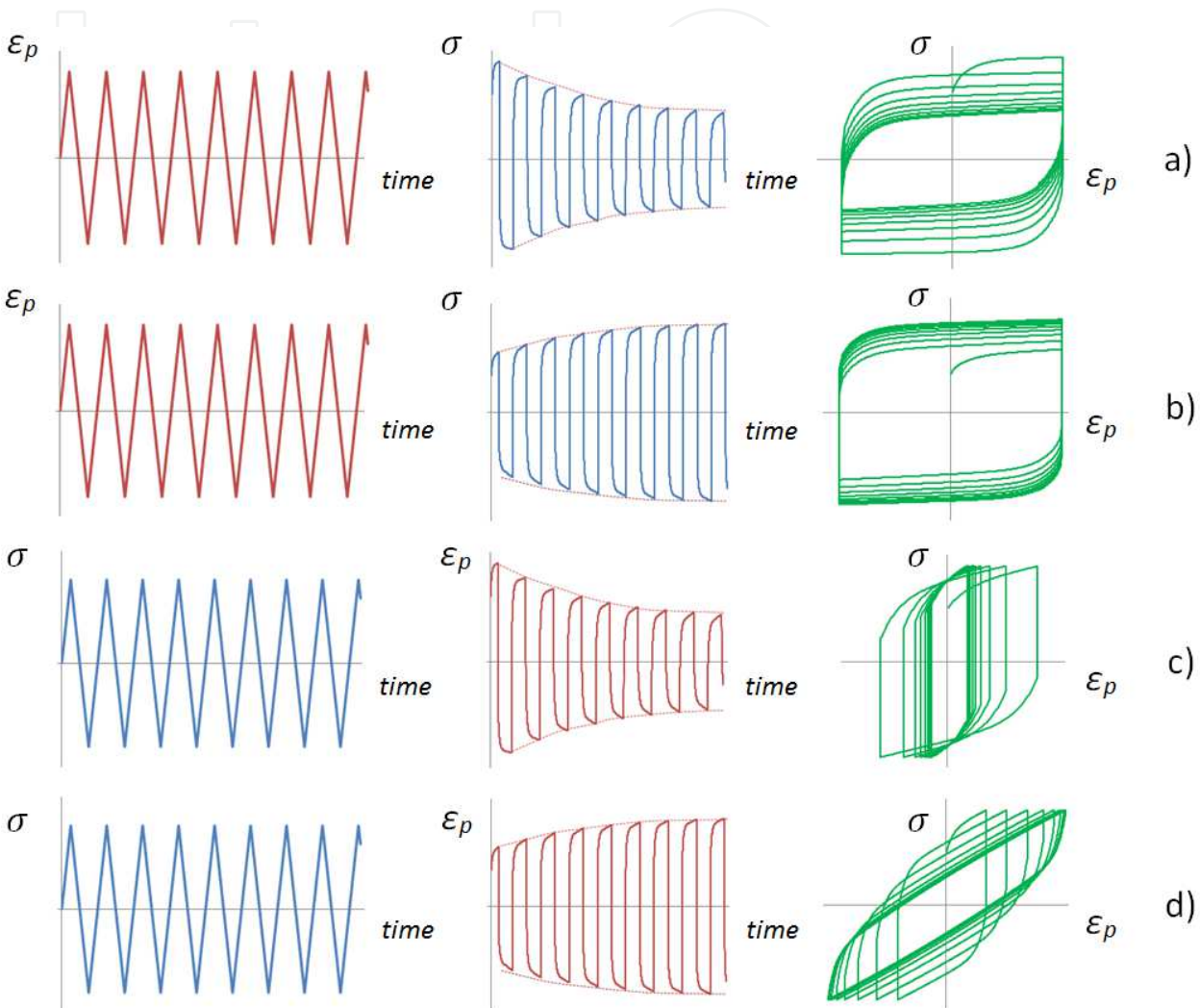

Fig. 2. Uniaxial fatigue test material response: Cyclic softening a) and cyclic hardening b) under plastic strain controlled loading and cyclic hardening c) and cyclic softening d) under stress controlled loading.

Some materials show very strong cyclic softening/hardening (stainless steels, cooper, etc.) some less obvious (structural steels). There can be also notable cyclic hardening in certain cycles range and in the remaining lifetime cyclical softening. Properties of cyclic hardening/softening don't depend only on material microstructure, but also on loading amplitude or more generally on previous strain history. Such transient behaviour of material makes accurate stress-strain modelling more difficult. There is very often mentioned possibility of transient stress-strain behaviour estimation according to its strength limit and yield limit ratio, but also very simple hypothesis is used, claiming that hard material cyclically softens whereas soft material cyclically hardens.

From upper peaks of several hysteresis loops corresponding to half lifetime is possible to obtain cyclic strain curve (Fig.3), which is often used in engineering computations.
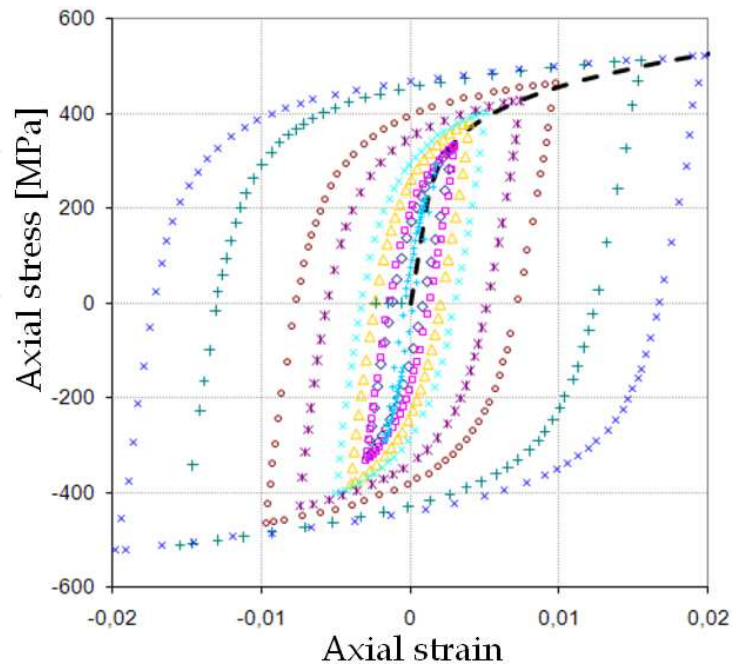

Fig. 3. Cyclic stress-strain curve of ST52 steel.

2.3 Non-masing behaviour

A material obeys Masing behaviour when the upper branches of hysteresis loops with different strain ranges after alignment in lower peaks overlap. More accurately, in the ideal case, single solid curve is created. From microscopic point of view Masing behaviour indicates stable microstructure in fatigue process. Most steel materials haven't Masing behaviour. Some engineering materials show Masing behaviour under certain testing conditions (Jiang & Zhang, 2008). As can be seen from the Fig.4, where the upper branches of hysteresis loops of the investigated material are displayed, the non-Masing behaviour is dependent on the amplitude of plastic strain ε_{ap}.
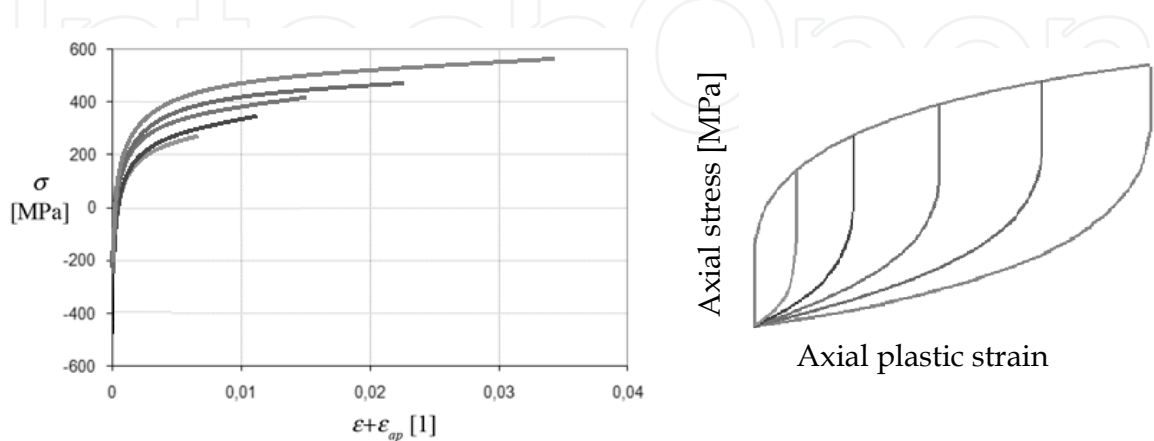

Fig. 4. Non-Masing's Behaviour of ST52 steel and schematic representation of Masing's Behaviour.

2.4 Non-proportional hardening

The Figure 5 illustrates the basic types of loading in the stress space. The tension-compression and simple shear belongs to the category of proportional loading, because there is no change of principal stress directions. This group also includes multi-axialloading in which the stress tensor components change proportionally. Non-proportional loading can be therefore defined as a loading that does not meet the specified condition, and is generally characterized by the loading path in the form of curve (Fig. 5).
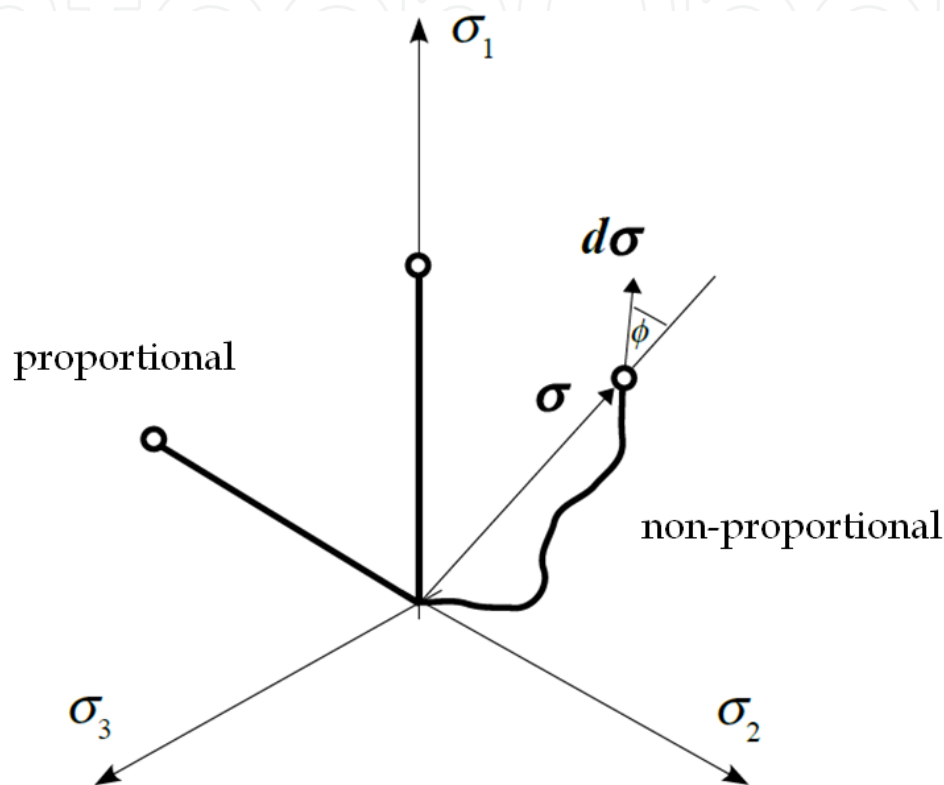

Fig. 5. Loading paths for non-proportional and proportional loading.

Conception of non-proportional hardening represents material hardening as a result of non-proportional loading. Most often it is investigated under tension-compression/torsion loading. Generally, the non-proportional hardening depends on material and shape of loading path. Thereafter we can express stress amplitude

$$\sigma_a(\Phi)=(1+\alpha\Phi)\ \sigma_a^p\ , \qquad (1)$$

where σ_a^p is the equivalent stress amplitude under proportional loading, whereas the influence of loading path shape in a cycle is involved in the non proportional parameter Φ and the material parameter of additional hardening is define as

$$\alpha= \sigma_a^n\ /\ \sigma_a^p - 1 \qquad (2)$$

where the quantity σ_a^n is the maximum value of von Mises equivalent stresses under non-proportional deformation (circular path). The equivalent stress amplitude is the radius of the minimum circle that circumscribes the loading path in the deviatoric stress space, see Fig.6.
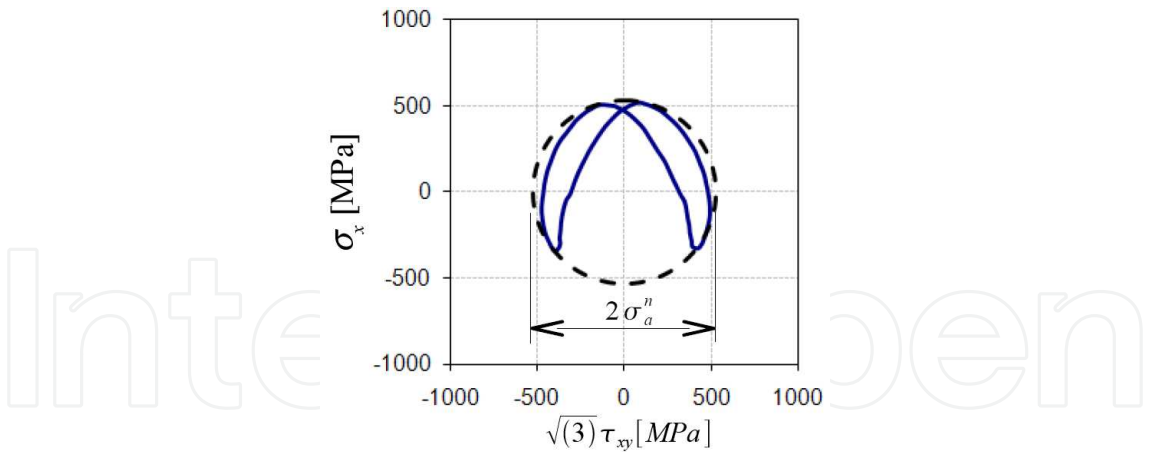
Fig. 6. Definition of equivalent stress amplitude under non-proportional loading.

Non-proportional hardening of FCC alloys pertinents to the stacking fault energy. For strain controlled 90° out-of-phase loading (circular path) it was found out, that the material parameter of non proportional strain hardening is higher for materials with lower value of the stacking fault energy (Doquet & Clavel, 1996).

2.5 Ratcheting

In an uniaxial test under load controll with non-zero mean stress σ_m the accumulation of axial plastic strain can occur cycle by cycle. This effect is called cyclic creep or ratcheting, see Fig.7. The uniaxial ratcheting is characterised by an open hysteresis loop and it is a result of different nonlinear behaviour of the material in tension and compression. The accumulation of plastic strain in initial cycles depends on the cyclic hardening/softening behaviour.
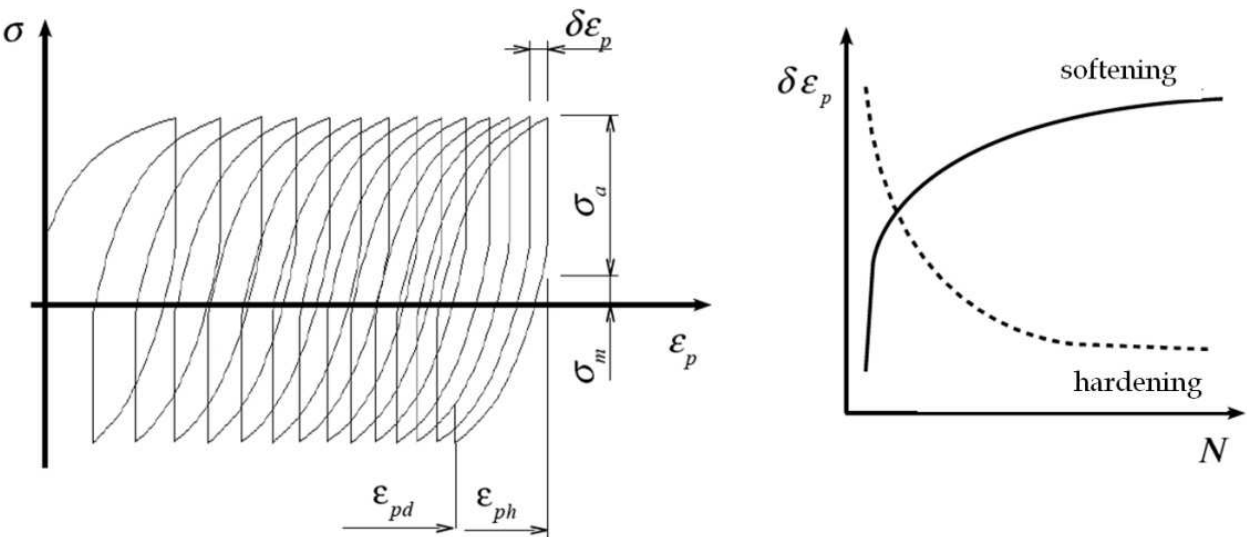

Fig. 7. Scheme of uniaxial ratcheting and influence of hardening/softening behaviour.

Generally, the ratcheting effect can be described as an accumulation of any component of strain tensor with increasing number of cycles. From the practical point of view the research of ratcheting, which occurs under multiaxial stress states, is also very important. There has been investigated mainly the multiaxial ratcheting under combined tension-

compression/torsion loading or the biaxial ratcheting caused by internal/external pressure with simultaneous cyclic tension-compression, bending or torsion. The ratcheting strain corresponds to the stress component with non-zero mean stress. The typical example is thin-walled tube subjected to internal (external) pressure and cyclic axial tension (Fig.8c,d). For pure symmetrical bending case (a) it was experimentally observed, that the cross-section becomes more and more oval with increasing number of cycles. This process is then strengthened, when the external pressure is applied too (b).
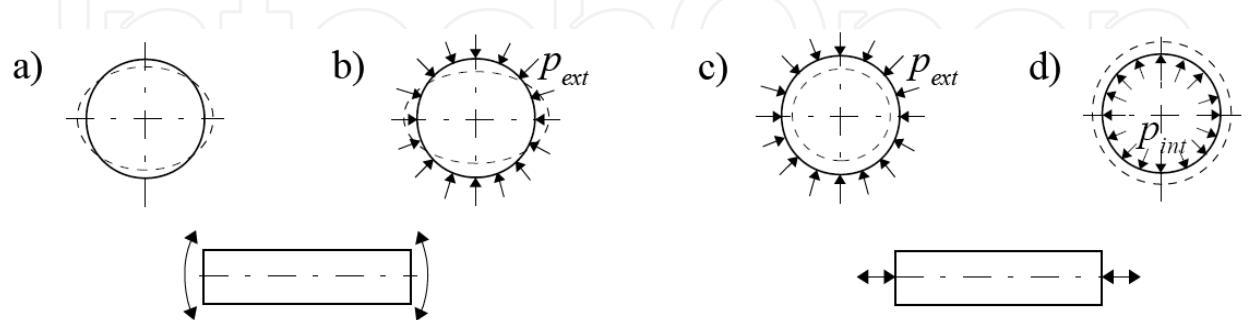

Fig. 8. Ratcheting of a piping component due to a) pure bending, b) bending and external pressure, c) external pressure and push-pull and d) internal pressure and push-pull.

As a next sample results of the fatigue test realised under tension – compression and torsion can serve (Fig.9). The test simulates ratcheting of shear strain, which occurs in surface layer subjected to rolling/sliding contact loading and was proposed by (McDowell, 1995). In the both axes force control was used. For measuring the axial and shear strain during the fatigue test two strain gauges rosette HBM RY3x3/120 were glued to the specimen. The pulsating torque leads to the accumulation of shear strain in the direction of applied torsional moment. The tested material R7T steel becomes almost elastic in initial cycles and then shows significant softening behaviour. After two hundred of loading cycles steady state is reached and the ratcheting rate is constant.
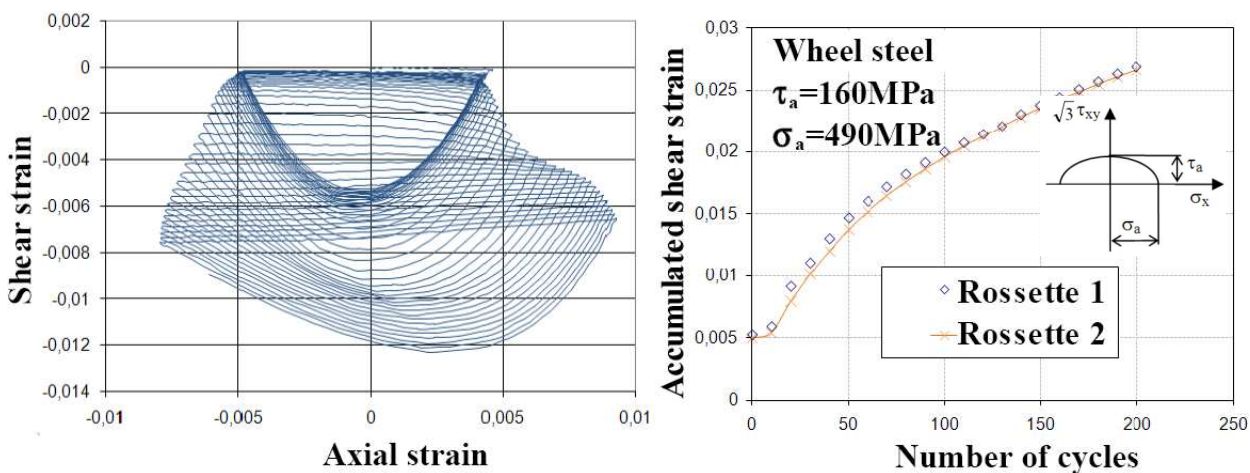

Fig. 9. Ratcheting of shear strain in the McDowell´s tension/torsion test.

A lot of rail and wheel steels show the decreasing ratcheting rate with the increasing number of cycles, which complicates accurate modelling of ratcheting effect. Ratcheting makes also life prediction of fatigue crack initiation difficult as well because the material

could fail due to the fatigue or to the accumulation of a critical unidirectional plastic strain (ratcheting failure).

2.6 Other effects in cyclic plasticity

From the theory of elasticity and strength it is well known that the yield locus of ductile materials can be described by an ellipse in the diagram shear stress - normal stress. However, through experiments carried out under uniaxial loading was found (Williams & Svensson, 1971), that if the specimen is loaded by torsion prior to tensile test, then the yield locus (yield surface) has deformed shape. The anisotropy is usually neglected in cyclic plasticity modelling. All of the reported effects of cyclic plasticity are dependent on temperature. With increasing temperature is also strengthened the influence of strain rate on the material response.

3. Constitutive modelling

Basically, cyclic plasticity models can be devided into these groups:

Overlay models (Besseling, 1958)
Single surface models (Armstrong&Frederick, 1966)
Multisurface models (Mroz, 1967)
Two-surface models (Dafalias&Popov, 1976)
Endochronicmodels (Valanis, 1971)
Models with yield surface distortion (Kurtyka, 1988)

Due to its wide popularity and robustness we focus only to the group of models with a single yield surface based on various evolution equations for internal variables.

3.1 Basics of incremental theory of plasticity

The elastoplasticity theory is based on the observations found in the case of uniaxial loading (Fig.10). The rate-independent material's behaviour model includes the additive rule, i.e. the total strain tensor

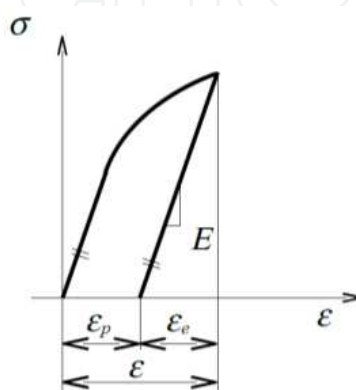$$\boldsymbol{\varepsilon} = \boldsymbol{\varepsilon}^e + \boldsymbol{\varepsilon}^p \qquad (3)$$

Fig. 10. Decomposition of total strain under uniaxial loading.

is composed of the plastic strain tensor ε^p and the elastic strain tensor ε^e. The second consideration is that stresses and elastic strains are subjected to Hook's law

$$\boldsymbol{\sigma} = \mathbf{D}^e : \boldsymbol{\varepsilon}^e = \mathbf{D}^e : \left(\boldsymbol{\varepsilon} - \boldsymbol{\varepsilon}^p \right) , \tag{4}$$

where $\mathbf{D}^e$ is the elastic stiffness matrix and the symbol ":" is contraction, i.e. using Einstein summation convention $d_{ij} = B_{ijkl} c_{kl}$.

In the uniaxial case, the development of irreversible deformation occurs due to crossing the yield limit σ_Y. Under multiaxial stress state it is necessary to consider an appropriate yield condition. For metallic materials the von Mises condition is mostly used

$$f = \sqrt{\frac{3}{2}(\mathbf{s} - \mathbf{a}):(\mathbf{s} - \mathbf{a})} - Y = 0 , \quad Y = \sigma_Y + R \tag{5}$$

where $\mathbf{s}$ is the deviatoric part of stress tensor $\boldsymbol{\sigma}$, $\mathbf{a}$ is the deviatoric part of back-stress $\boldsymbol{\alpha}$, which states the centre position for the yield surface with the initial size σ_Y and R is the isotropic internal variable. The contraction operation ":" in (5) can be expressed again in terms of Einstein summation convention $d = b_{ij} c_{ij}$. Now it is necessary to answer the question: When happens a change of plastic strain increment? If the point representing the current stress state lies on the yield surface it can be supposed that this point do not leave the yield surface, the so called consistency condition $\dot{f} = 0$ must be valid. In case of active loading

$$f = 0, \quad \dot{f} = 0 \text{ and } \frac{\partial f}{\partial \boldsymbol{\sigma}} : d\sigma \geq 0 , \tag{6}$$

the plastic deformation development is directed by the associated plastic flow rule

$$d\boldsymbol{\varepsilon}^p = \sqrt{\frac{3}{2}} d\lambda \frac{\partial f}{\partial \boldsymbol{\sigma}} , \quad \frac{\partial f}{\partial \boldsymbol{\sigma}} = \sqrt{\frac{3}{2}} \frac{\mathbf{s} - \mathbf{a}}{Y} = \mathbf{n} , \tag{7}$$

where the plastic multiplier $d\lambda$ in (7) corresponds to the equivalent plastic strain increment

$$dp = \sqrt{\frac{2}{3} d\boldsymbol{\varepsilon}^p : d\boldsymbol{\varepsilon}^p} . \tag{8}$$

In this concept of single yield surface, the kinematic hardening rule

$$d\mathbf{a} = g\left(\mathbf{a}, \dot{\boldsymbol{\varepsilon}}^p, d\dot{\boldsymbol{\varepsilon}}^p, dp, \mathbf{n}, etc. \right) \tag{9}$$

and the isotropic hardening rule

$$dY = h\left(R, dp, \boldsymbol{\sigma}, \mathbf{a}, \dot{\boldsymbol{\varepsilon}}^p, etc. \right) \tag{10}$$

play an essential role for the robustness of stress-strain model response. When the both hardening rules are used we speak about mixed hardening. Transient effects from initial cycles (cyclical hardening/softening), non-proportional hardening, ratcheting and other

effects of cyclic plasticity can be described by a suitable superposition of kinematic and isotropic hardening rules.

In the case of cyclic loading a kinematic hardening rule should always be included in the plasticity model, otherwise the Bauschinger's effect cannot be correctly described.
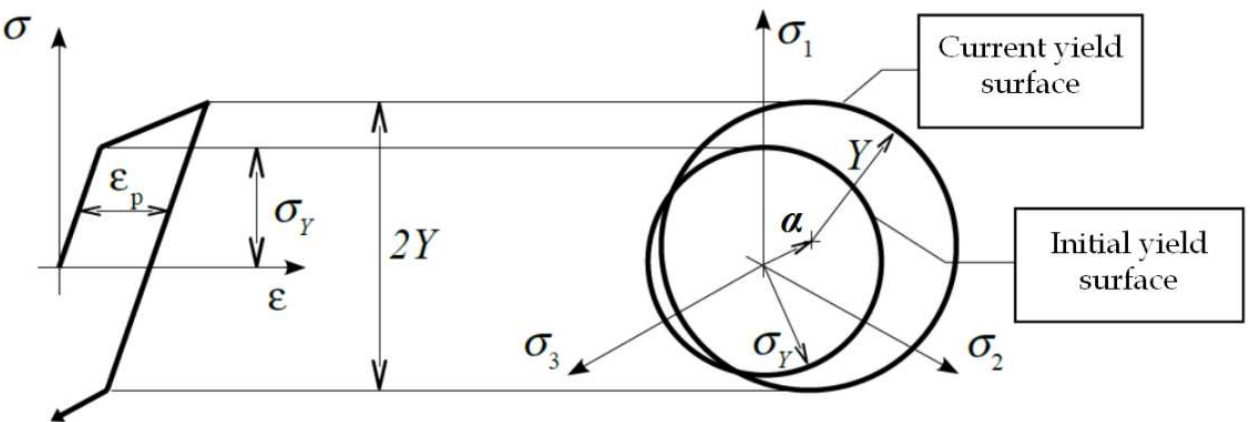

Fig. 11.Von Mises yield function with mixed hardening in the deviatoric plane.

The kinematic hardening rule is important in terms of the needs of capturing the cyclical response of the material. Description of the classical kinematic hardening rules and the resulting cyclic plasticity models is contained in next four subsections. Their availability in selected commercial software based on finite element method is given in Table 1.

Kinematic hardening	Ansys 13	Abaqus	MSC.Marc	MSC. Nastran
Bilinear	x (Prager)	x	x (Ziegler)	x (Ziegler)
Multilinear	x (Besseling)	-	-	-
Armstrong-Frederick	x	x	x	x
Chaboche	x (M_{max}=5)	x (M_{max}=3)	-	-

Table 1.Occurrence of cyclic plasticity models in some popular FE software.

3.2 Bilinear and multilinear kinematic hardening models

There are two bilinear kinematic hardening rules coded in the most popular FE software, suggested by Prager (1953) and Ziegler (1959). The models predict the same response for von Mises material (Ottosen&Ristinmaa, 2005) and for uniaxial loading their response is bilinear. The models show no ratcheting under uniaxial loading and tend to plastic shakedown for a biaxial history of loading. The nonlinearity in stress-strain behaviour can be introduced by a multisurface model, when each surface represents a constant work hardening modulus in the stress space (Mroz, 1967).

Besseling in 1958 introduced a multilinear overlay model, which has a physical meaning and does not use any notion of surfaces. The Besseling model predicts plastic shakedown for

uniaxial loading independently of mean stress value. Unfortunately, the mean stress relaxation effect cannot be described too.

3.3 Armstrong-Frederick kinematic hardening model

The important work, leading to the introduction of nonlinearity in the kinematic hardening rule, was the research report of Armstrong and Frederick (1966). In their model the memory term is added to the Prager rule

$$d\boldsymbol{\alpha} = \frac{2}{3}Cd\boldsymbol{\varepsilon}_p - \gamma\boldsymbol{\alpha}dp \tag{11}$$

where C and γ are material parameters. Their physical meaning will be explained for push-pull loading. The quantity dp is an increment of accumulated plastic strain, which is expressed as follows

$$dp = \sqrt{\frac{2}{3}d\boldsymbol{\varepsilon}_p : d\boldsymbol{\varepsilon}_p} \tag{12}$$

Considering initially isotropic homogenous material, Von-Misses condition can be again used as follows

$$f = \sqrt{\frac{3}{2}(\boldsymbol{s} - \boldsymbol{a}):(\boldsymbol{s} - \boldsymbol{a})} - \sigma_Y \tag{13}$$

where $\boldsymbol{a}$ is a deviator of backstress $\boldsymbol{\alpha}$ and $\boldsymbol{s}$ is deviator of stress tensor $\boldsymbol{\sigma}$.

For the uniaxial loading case, the von Mises yield condition becomes to the simpler form

$$f = |\sigma - \alpha| - \sigma_Y = 0 \tag{14}$$

Similarly we can modify nonlinear kinematic hardening rule if we will consider only deviatoric part of the equation (11) taking into account plastic incompressibility.

Then the nonlinear kinematic hardening rule leads to the differential equation

$$d\alpha = Cd\varepsilon_p - \gamma\alpha|d\varepsilon_p| \tag{15}$$

Now, we can use a multiplier $\psi = \pm 1$ to dispose of the absolute value

$$d\alpha = Cd\varepsilon_p - \gamma\alpha|d\varepsilon_p| = Cd\varepsilon_p - \gamma\alpha\psi d\varepsilon_p = (C - \gamma\alpha\psi)d\varepsilon_p \tag{16}$$

separate variables

$$\int_{\alpha_0}^{\alpha} \frac{d\alpha}{C - \gamma\alpha\psi} = \int_{\varepsilon_0}^{\varepsilon} d\varepsilon_p \tag{17}$$

and integrate to get the equation for backstress evolution

$$\alpha = \psi \frac{C}{\gamma} + \left(\alpha_0 - \psi \frac{C}{\gamma} \right) e^{-\psi \gamma \left(\varepsilon_p - \varepsilon_{p0} \right)} \tag{18}$$

Therefore, the relation for stress is given by yield condition

$$\sigma = \alpha + \psi \sigma_Y \tag{19}$$

For tension $\psi = 1$ and considering zeros initial values of plastic strain and backstress this equation is given

$$\sigma = \sigma_Y + \frac{C}{\gamma} \left(1 - e^{-\gamma \varepsilon_p} \right) \tag{20}$$

Now, we can investigate the limit values of the nonlinear function and its first derivation to get a concept about influence of parameters C and γ on stress – strain response of the Armstrong-Frederick model

$$\lim_{\varepsilon_p \to 0} C e^{-\gamma \varepsilon_p} = C \tag{21}$$

$$\lim_{\varepsilon_p \to \infty} \sigma_Y + \frac{C}{\gamma} \left(1 - e^{-\gamma \varepsilon_p} \right) = \sigma_Y + \frac{C}{\gamma} \tag{22}$$
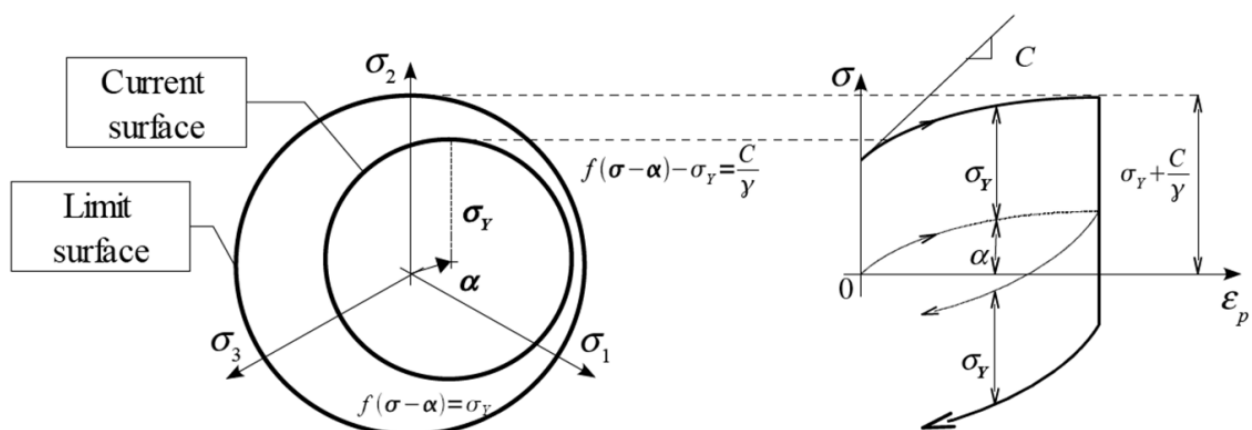

Fig. 12. Properties of the nonlinear kinematic hardening model of Armstrong/Frederick.

Described nonlinear kinematic hardening model allows to correctly capture Bauschinger effect and even behavior by nonsymmetrical loading in tension-compression. The large advantage of Armstrong-Frederick model is its easy implementation and the mentioned nonlinear behavior of the model. On the other hand, the model can not descibe the hysteresis loop shape precisely.

For the case of cyclic loading the parameters σ_Y, C and γ should be estimated from the cyclic strain curve. It is possible to determine the equation corresponding to the cyclic curve of Armstrong-Frederick model by application of equation (18) for the upper branch and the bottom branch of hysteresis loop. For tension $\psi = 1$ is valid and we have

$$\alpha_{\max} = \frac{C}{\gamma} + \left(\alpha_{\min} - \frac{C}{\gamma} \right) e^{-\gamma \left(\varepsilon_p - \varepsilon_{ap} \right)} \tag{24}$$

For the compression ($\psi = -1$) similarly

$$\alpha_{\min} = -\frac{C}{\gamma} + \left(\alpha_{\max} + \frac{C}{\gamma} \right) e^{\gamma \left(\varepsilon_p - \varepsilon_{ap} \right)} \tag{25}$$

After substitution of (24) to the equation (25) we get

$$\sigma_a = \sigma_Y + \frac{C}{\gamma} \tanh \left(\gamma \varepsilon_{ap} \right) \tag{26}$$

where tanh(x) is the hyperbolic tangent function and σ_a, ε_{ap} are stress amplitude and plastic strain amplitude respectively.
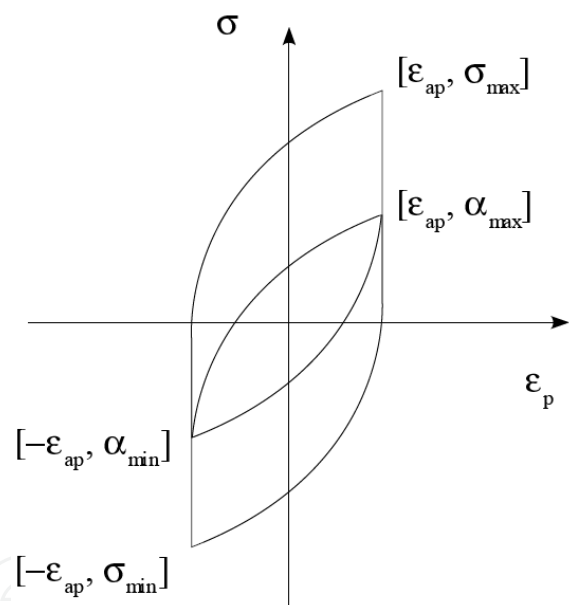
Fig. 13. Initial conditions for the backstress and plastic strain.

For a proper ratcheting description, the condition of equality for computed and experimentally stated ratcheting strain rate for opened stabilized hysteresis loop (Fig.7) should be satisfied

$$\delta \varepsilon_{pFEM} = \delta \varepsilon_{pEXP} \tag{27}$$

According to (Chaboche & Lemaitre, 1990), for Armstrong-Frederick kinematic hardening rule the plastic strain increment per cycle can be written as follows (with absence of isotropic hardening)

$$\delta\varepsilon_{pFEM} = \frac{1}{\gamma} \cdot \ln\left[\frac{\left(\frac{C}{\gamma}\right)^2 - (\sigma_{\min} + \sigma_Y)^2}{\left(\frac{C}{\gamma}\right)^2 - (\sigma_{\max} + \sigma_Y)^2}\right] \quad (28)$$

where $\delta\varepsilon_p$ is measured between upper peaks of two hysteresis loops as can be seen in Fig.7.

3.4 Chaboche kinematic hardening model

Very important improvement was the proposal of nonlinear kinematic hardening model by Chaboche (1979), which eliminated Armstrong-Frederick model disadvantages by creating a backstress through superposition of M parts

$$a = \sum_{i=1}^{M} a^{(i)} \quad (29)$$

whereas for each part the evolution equation of Armstrong and Frederick is used

$$da^{(i)} = \frac{2}{3}C_i d\varepsilon_p - \gamma_i a^{(i)} dp \quad (30)$$

where C_i and γ_i are material parameters.

Due to the usage of Armstrong-Frederick evolution law we can directly write the expression for static strain curve

$$\sigma = \psi\sigma_Y + \sum_{i=1}^{M} \psi\frac{C_i}{\gamma_i} + \left(\alpha_0^{(i)} - \psi\frac{C_i}{\gamma_i}\right)e^{-\psi\gamma_i(\varepsilon_p - \varepsilon_{p0})} \quad (31)$$

and for cyclic strain curve

$$\sigma_a = \sigma_Y + \sum_{i=1}^{M} \frac{C_i}{\gamma_i}\tanh\left(\gamma_i\varepsilon_{ap}\right) \quad (32)$$

The quality of cyclic strain curve description is adequate in the case of Chaboche model with the three evolution parts.

Thanks to the similar properties of functions tanh(x) and 1-exp(-x), including its derivatives, it is possible to use the same approach for parameter estimation from the static even cyclic strain curve. Parameters should be determined for example by a nonlinear least-squares method. It is useful to consider Prager's rule for the last backstress part ($\gamma_M = 0$). The parameter influence ratcheting and mean stress relaxation effects. Therefore, we can use this approximation function for cyclic and static strain curves respectively

$$\sigma_a = \sigma_Y + \sum_{i=1}^{M-1} \frac{C_i}{\gamma_i}\tanh\left(\gamma_i\varepsilon_{ap}\right) + C_M\varepsilon_{ap} \quad (33)$$

$$\sigma_a = \sigma_Y + \sum_{i=1}^{M-1} \frac{C_i}{\gamma_i}\left(1 - e^{-\gamma_i \varepsilon_p}\right) + C_M \varepsilon_p \tag{34}$$

When the cyclic strain curve of the investigated material is not available, it is possible to use for the calibration of the model also large saturated hysteresis loop. Based on the relationship (31), considering tension ($\psi = 1$) and these initial values (see Fig15)

$$\alpha_0^{(i)} = -\frac{C_i}{\gamma_i}, \varepsilon_{p0} = -\varepsilon_{ap} \tag{35}$$

we can get for the upper branch of the hysteresis loop this expression

$$\sigma = \sigma_Y + \sum_{i=1}^{2} \frac{C_i}{\gamma_i}\left(1 - 2e^{(-\gamma_i \varepsilon_p - (-\varepsilon_{ap}))}\right) + C_3 \varepsilon_p \tag{36}$$

In the Chaboche model the parameter γ_M influences ratcheting (provided that the last backstress part has the lowest value of the parameter γ_i) and is chosen to be small (up to γ_M=10). For the case of γ_M= 0 ratcheting cannot occur. However, after particular number of cycles the stabilized hysteresis loop will be formed (the Chaboche model tends to plastic shakedown) as it is clear from the graph at the Fig.16. For many materials such behavior does not correspond with reality and during numerical modeling, constant deformation increment can be achieved with aim of suitable choice of parameter γ_M. We can also provide the relation

$$\gamma_M = \frac{\delta \varepsilon_p \cdot C_M}{2 \cdot \sigma_m \cdot \Delta \varepsilon_p}, \tag{37}$$

published elsewhere (Chaboche and Nouailhas 1989).

Thus, with suitable choice of γ_M we get very good model for uniaxial ratcheting prediction (ratcheting with steady state only). In case of non-proportional loading the Chaboche model with three backstresses (*M*=3) considered in Fig.14 and Fig.15 drastically over predicts ratcheting as has been shown by other researchers (Bari & Hassan, 2000).
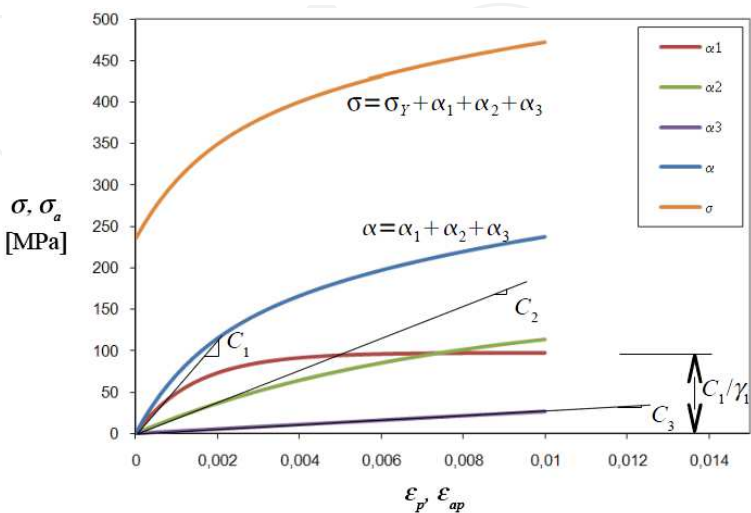

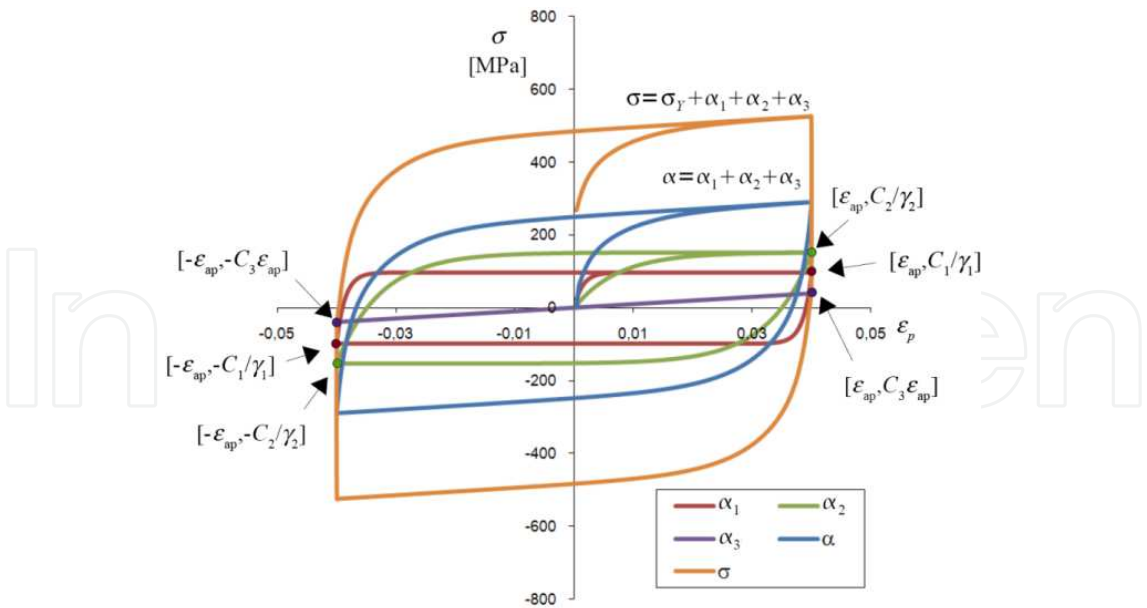Fig. 14. Properties of constants of Chaboche nonlinear kinematic hardening model (case *M*=3).

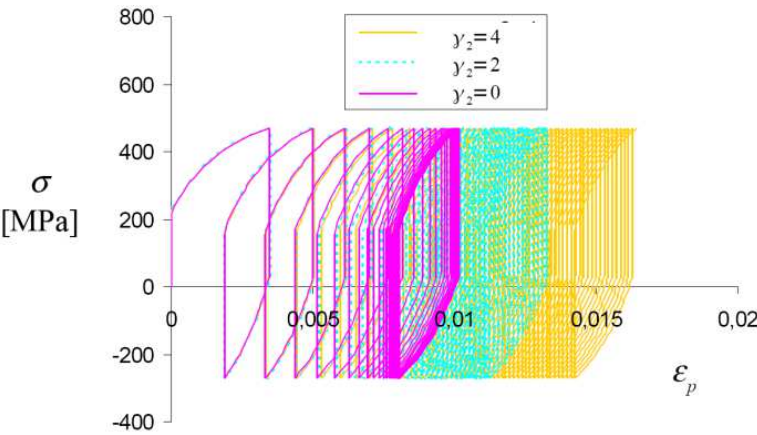Fig. 15. Scheme for use of the hysteresis loop to identify parameters of Chaboche model.

Fig. 16. Influence of parameter γ_2 on ratcheting response of the Chaboche model (*M*=2).

3.5 Mixed hardening models

Most of materials exhibit Masing and cyclic softening/hardening behaviour, which can be described by superposition of isotropic hardening to a kinematic hardening rule. In this case the size of yield surface *Y* is expressed with aim of initial value of σ_Y and isotropic variable *R*, which is usually dependent on the accumulated plastic deformation.

If we would like to describe cyclic softening/hardening, it is convenient to use simple evolutionary equation, leading to nonlinear isotropic hardening rule

$$dR = b(R_\infty - R)dp \tag{38}$$

where R_∞, *b* are material parameters and *dp* is an increment of accumulated plastic strain. The value of constant *b*, which determines the rate of stabilization of the hysteresis loop in case of loading with constant strain amplitude (Fig.17), can be determined directly from following equation

$$R = R_\infty (1 - e^{-b \cdot p})$$ (39)

which follows from integration of equation (39) under following assumption: Change of variable R from zero to R_∞ and p from zero to p. Other possibilities how to identify the constant b are briefly described in (Chaboche & Lemaitre, 1990).
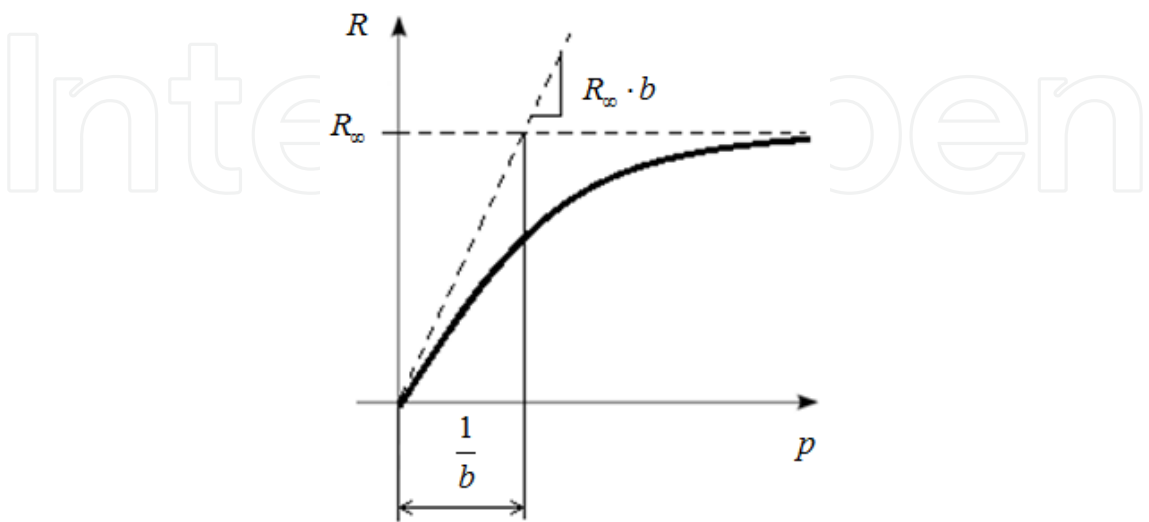

Fig. 17. Evolution of isotropic internal variable R for the nonlinear isotropic hardening rule.

The material parameter R_∞ can be determined, for example, by comparison of static and cyclic strain curve of particular material.

3.6 Other cyclic plasticity models

After Chaboche (1979) there were designed many evolution equations for better ratcheting prediction in the category of nonlinear kinematic hardening rules, but mostly based on the Chaboche superposition of several backstress parts. Because of the large number of theories we choose for their presentation form of table, which contains links to the original publications (Table 2). Presented group of cyclic plasticity models of Chaboche type, which considers the backstress to be defined by M parts

$$d\mathbf{a} = \sum_{i=1}^{M} d\mathbf{a}^{(i)}$$ (40)

can be generalized considering the evolution equation in the form

$$d\mathbf{a}^{(i)} = \frac{2}{3} C_i d\boldsymbol{\varepsilon}^p - \gamma_i \mathbf{a}^{(i)} dp^{(i)}$$ (41)

where C_i, γ_i are material parameters, $d\boldsymbol{\varepsilon}^p$ is plastic strain increment and $dp^{(i)}$ is the increment of accumulated plastic strain causing dynamic recovery of $\alpha^{(i)}$.

Authors do not guarantee completeness of the set of theories. There are also some new models and approaches. Very progressive are so called models with yield surface distortion, for example Vincent (2004), which are able to model the anisotropy induced by previous plastic deformation (see chapter 2.6).

	Proposed modification	Authors
1.	$$\boldsymbol{a}^{(i)}dp^{(i)}=\left(\boldsymbol{a}^{(i)}:\frac{\partial f}{\partial \boldsymbol{\sigma}}\right)\frac{\partial f}{\partial \boldsymbol{\sigma}}dp\,,$$	Burlet-Cailletaud 1986
2.	$$dp^{(i)}=dp \ \text{ for } i=1,2,3$$ $$dp^{(i)}=\left\langle 1-\frac{\bar{a}_i}{f(\alpha_i)}\right\rangle dp \ \text{ for } i=4, \ f(\alpha_i)=\sqrt{\frac{3}{2}\boldsymbol{a}^{(i)}:\boldsymbol{a}^{(i)}}$$	Chaboche 1991, 1994
3.	$$dp^{(i)}=H(f_i)\left\langle \boldsymbol{d}\boldsymbol{\varepsilon}_p:\frac{\boldsymbol{a}^{(i)}}{\bar{a}_i}\right\rangle,$$ where $\bar{a}_i=\sqrt{\frac{3}{2}\boldsymbol{a}^{(i)}:\boldsymbol{a}^{(i)}}$, $f_i=\bar{a}_i^2-(\frac{c_i}{\gamma_i})^2$ and $H(f_i)$ denotes Heavyside step function.	Ohno-Wang 1993
4.	$$dp^{(i)}=\left(\frac{\bar{a}_i}{C_i/\gamma_i}\right)^{m_i}\left\langle \boldsymbol{d}\boldsymbol{\varepsilon}_p:\frac{\boldsymbol{a}^{(i)}}{\bar{a}_i}\right\rangle,$$	Ohno-Wang 1993
5.	$$dp^{(i)}=\left(\frac{\bar{a}_i}{C_i/\gamma_i}\right)^{m_i}\left\langle \boldsymbol{d}\boldsymbol{\varepsilon}_p:\frac{\boldsymbol{a}^{(i)}}{\bar{a}_i}\right\rangle, \ m_i=A_i\left\langle \frac{d\boldsymbol{\varepsilon}_p}{dp}:\frac{\boldsymbol{a}^{(i)}}{\bar{a}_i}\right\rangle^{B_i}$$	McDowell 1995
6.	$$dp^{(i)}=\left(\frac{\bar{a}_i}{C_i/\gamma_i}\right)^{m_i}dp\,,$$ $$m_i=A_{0i}\left(2-\frac{d\boldsymbol{\varepsilon}_p}{dp}:\frac{\boldsymbol{a}^{(i)}}{\bar{a}_i}\right), \ A_{0i}=Q_i\left(1+a_\chi e^{b_\chi R_M}\right),$$	Jiang-Sehitoglu 1996
7.	$$dp^{(i)}=\left[\mu_i+H(f_i)\left\langle \frac{\partial f}{\partial \boldsymbol{\sigma}}:\frac{\boldsymbol{a}^{(i)}}{C_i/\gamma_i}-\mu_i\right\rangle\right]dp\,,$$	Abdel-Karim / Ohno 2000
8.	$$\boldsymbol{a}^{(i)}dp^{(i)}=\left[\delta'\boldsymbol{a}^{(i)}+(1-\delta')\left(\boldsymbol{a}^{(i)}:\frac{\partial f}{\partial \boldsymbol{\sigma}}\right)\frac{\partial f}{\partial \boldsymbol{\sigma}}\right]dp\,, \ \text{(pro } i=1,2,3)$$ $$\boldsymbol{a}^{(i)}dp^{(i)}=$$ $$=\left[\delta'\boldsymbol{a}^{(i)}+(1-\delta')\left(\boldsymbol{a}^{(i)}:\frac{\partial f}{\partial \boldsymbol{\sigma}}\right)\frac{\partial f}{\partial \boldsymbol{\sigma}}\right]\left\langle 1-\frac{\bar{a}_i}{f(\alpha_i)}\right\rangle dp\,, \ \text{(pro } i=4)$$	Bari a Hassan 2002
9.	$$\boldsymbol{a}^{(i)}dp^{(i)}=\left(\frac{\bar{a}_i}{C_i/\gamma_i}\right)^{\chi_i}dp-\frac{\boldsymbol{a}^{(i)}}{r_i}\dot{r}_i\,, \quad \dot{r}_i=b(r_i^T-r_i)\dot{p}\,,$$ $$r_i^T=r_i^0\left[1+\frac{a_i^1}{(1+b_1 p)^2}+\frac{a_i^2}{(1+b_2 p)^2}+\frac{a_i^3}{(1+b_3 p)^2}\right],$$ $$\chi_i=\left\langle \chi_i^0+(\chi_i^0+1)(c_i^\chi-1)\left(1-\left|\frac{\partial f}{\partial \boldsymbol{\sigma}}:\frac{\boldsymbol{a}^{(i)}}{\bar{a}_i}\right|\right)\right\rangle, \quad \chi_i^0=Q_i\left(1+\frac{a_\chi}{(1+b_\chi R_\varepsilon)^2}\right)$$	Döring 2003
10.	$$\boldsymbol{a}^{(i)}dp^{(i)}=$$ $$=\left(\frac{\bar{a}_i}{C_i/\gamma_i}\right)^{m_i}\left[\delta'\boldsymbol{a}^{(i)}+(1-\delta')\left(\boldsymbol{a}^{(i)}:\frac{\partial f}{\partial \boldsymbol{\sigma}}\right)\frac{\partial f}{\partial \boldsymbol{\sigma}}\right]\left\langle \boldsymbol{d}\boldsymbol{\varepsilon}_p:\frac{\boldsymbol{a}^{(i)}}{\bar{a}_i}\right\rangle,$$ $$d\delta'=\beta(d\delta'_\infty-d\delta')dp\,.$$	Chen-Jiao 2004
11.	$$dp^{(i)}=\left[\mu_i+H(f_i)\left\langle \frac{\partial f}{\partial \boldsymbol{\sigma}}:\frac{\boldsymbol{a}^{(i)}}{C_i/\gamma_i}-\mu_i\right\rangle\right]dp\,,$$ $$\mu_i=\mu=\frac{\mu_0}{(1+a\Phi)}\,, \ \Phi=1-\sqrt{\frac{s:\dot{s}}{\bar{s}:\dot{\bar{s}}}}\,.$$	Kang-Gao-Yang 2004
12.	$$dp^{(i)}=\left\langle \frac{\partial f}{\partial \boldsymbol{\sigma}}:\frac{\boldsymbol{a}^{(i)}}{\bar{a}_i}\right\rangle^{\chi_i}\left(\frac{\bar{a}_i}{C_i/\gamma_i}\right)^{m_i}\left\langle \boldsymbol{d}\boldsymbol{\varepsilon}_p:\frac{\boldsymbol{a}^{(i)}}{\bar{a}_i}\right\rangle$$	Chen et al. 2005
13.	$$\boldsymbol{a}^{(i)}dp^{(i)}=H(f_i)\left\langle \boldsymbol{d}\boldsymbol{\varepsilon}_p:\frac{\boldsymbol{a}^{(i)}}{\bar{a}_i}\right\rangle \boldsymbol{a}^{(i)}+\xi_i(\bar{a}_i)^{m-1}\boldsymbol{a}^{(i)}\,,$$	Yaguchi - Takahashi 2005
14.	$$dp^{(i)}=\left[\mu_i+H(f_i)\left\langle \frac{\partial f}{\partial \boldsymbol{\sigma}}:\frac{\boldsymbol{a}^{(i)}}{C_i/\gamma_i}-\mu_i\right\rangle\right]dp\,, \quad \mu_i=\eta\left\langle \frac{\partial f}{\partial \boldsymbol{\sigma}}:\frac{\boldsymbol{a}^{(i)}}{\bar{a}_i}\right\rangle^\chi\,,$$ $$d\eta=d\eta_1+d\eta_2\,, \ d\eta_1=\omega_1(\eta_{\infty 1}-\eta_1)dp\,, \ d\eta_2=\omega_2(\eta_{\infty 2}-\eta_2)dp\,,$$ $$\chi=\chi_\infty+(\chi_0-\chi_\infty)e^{-\omega_\chi p}\,,$$	Halama 2007

Table 2. Overview of some kinematic hardening rules.

It is obvious that many theories differ very little. For correct description of ratcheting in proportional and non-proportional loading more and more authors introduced a non-proportional parameter, which enables simultaneous correct description of uniaxial and multiaxial ratcheting (Chen & Jiao 2004; Chen, 2005; Halama, 2008). Significant improvements of prediction capability can be reached by using memory surfaces (Jiang & Sehitoglu, 1996 and Döring, 2003). Presented models should be compared in terms of nonlinearity, established for each backstress in the case of uniaxial loading. The Fig.18 compares four basic hardening rules.

Common values of parameters are considered for models Ohno-Wang-II and AbdelKarim-Ohno in the Fig.18. Both models lead to the Ohno-Wang model I at a certain choice of parameters affecting ratcheting. In the case of the AbdelKarim-Ohno model this occurs when $\mu_i = 0$ for all i, see Fig.19. Ohno-Wang model II corresponds to the Ohno-Wang model I, if $m_i = \infty$ for all i. Thus, the nonlinearity in the Fig.18 is weak for common parameters (Ohno-Wang II: $m_i \gg 1$, AbdelKarim-Ohno: $\mu_i < 0.2$) and we can therefore use the same procedure for estimation of the parameters C_i, γ_i ($i = 1$, ...,M) as in the case of multilinear Ohno-Wang model I. For determination of these material parameters we can use again either cyclic strain curve of the material (Ohno-Wang, 1993), (AbdelKarim-Ohno, 2000), or a stabilised hysteresis loop (Bari & Hassan, 2000).
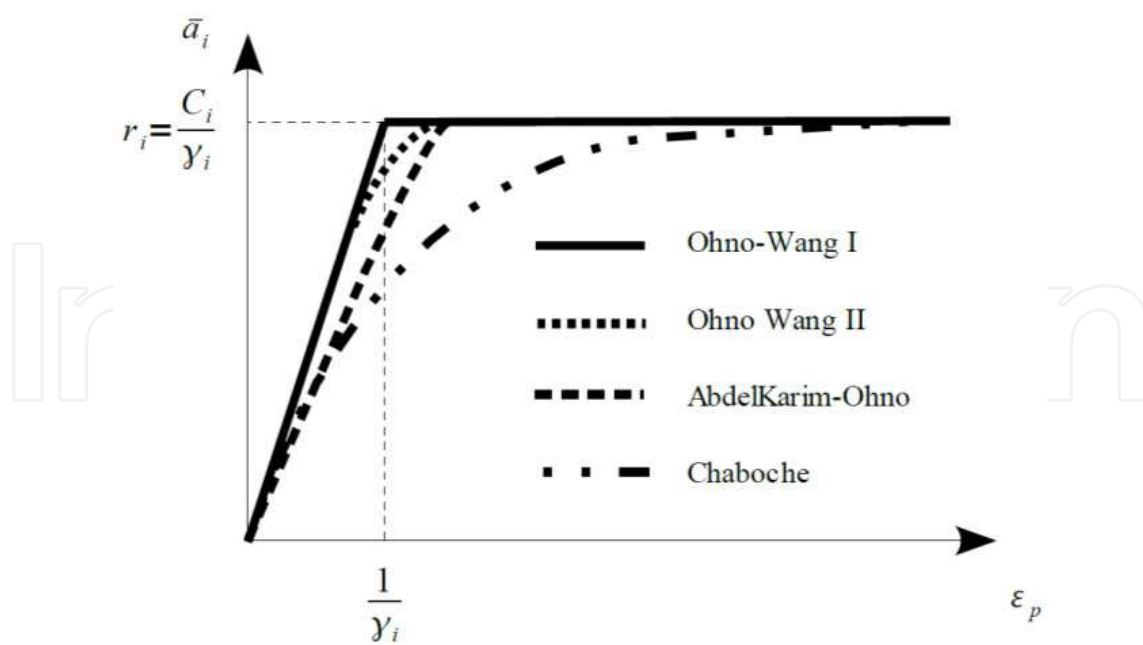
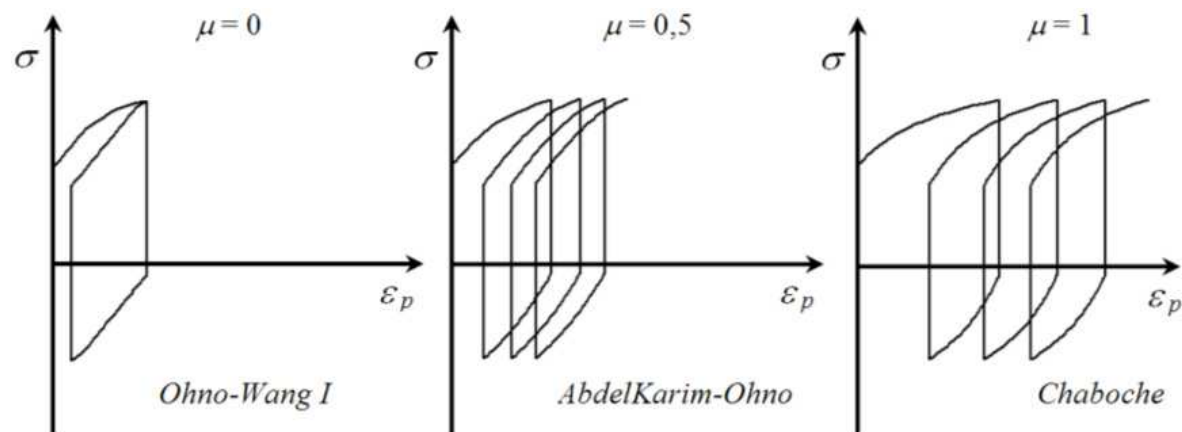Fig. 18. Nonlinearity introduced in four basic cyclic plasticity models.

Fig. 19. Influence of ratcheting parameter on the response of AbdelKarim-Ohno model.

As shown in Fig.19, appropriate choice of parameter gives desired ratcheting rate. Considering the only one parameter for ratcheting $\mu_i = \mu$ and its evolution by equation

$$d\mu = \omega\left(\mu_\infty - \mu\right)dp \qquad (42)$$

transient effects in initial cycles can be described too.

4. Ratcheting simulations for a wheel steel

There was realized a set of low-cycle fatigue tests of specimen made from R7T wheel steel at the Czech Technical University in Prague. The specimens were subjected to tension-compression and tension/torsion on the test machine MTS 858 MiniBionix. All tests were force controlled. More detailed description of experiments was reported elsewhere (Halama, 2009). Four cases considered for simulations in this book are shown in Fig.20.
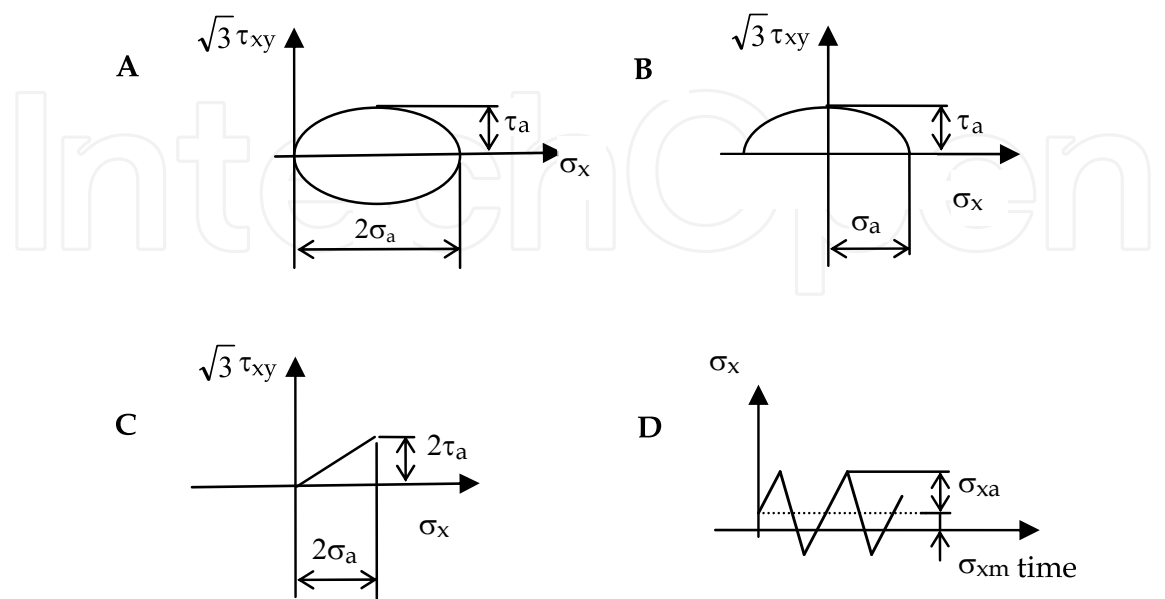
Fig. 20. The scheme of four realized loading paths.

For a description of the stress strain behaviour the AbdelKarim-Ohno model and two classical models of cyclic plasticity were chosen - Armstrong-Frederick model and Chaboche model with two backstress parts (*M*=2). The AbdelKarim-Ohno model was implemented to the ANSYS program via user subroutine. Material parameters used in simulations are listed in the tables below, except elastic constants (Young modulus E=180000MPa and Poisson´s ratio ν=0.3).

Plasticitymodel	Material parameters
Armstrong-Frederick and Voce rule (AF)	σ_Y=500 MPa, *C*=108939, γ=2.5 R_∞=-250MPa, *b*=30
Chabocheand Voce rule (CHAB)	σ_Y=500 MPa, C_1=264156, γ_1=873, C_2=20973, γ_2=1 R_∞=-320MPa, *b*=30
AbdelKarim-Ohno (AKO)	$\sigma_Y = 200MPa$ $C_{1-6} = 310600, 130770, 36290, 32420, 12940, 18350MPa$ $\gamma_{1-6} = 5884, 2020, 980, 520, 255, 3$ $\mu_0 = 0.5, \omega = 0.5, \mu_\infty = 0.14$

Table 3. Material parameters of used cyclic plasticity models.

Cyclic plasticity models were calibrated using saturated hysteresis loop from the test with strain range of 1.5% (Fig.21) and a uniaxial ratcheting test. The calibration procedure used for AbdelKarim-Ohno model was described in the paper Halama (2008). The results of ratcheting prediction gained from simulations of the low cycle fatigue test with nonzero mean stress (case D: 500 cycles with σ_m = 40MPa and σ_a = 500MPa) are shown for all three material models in Fig. 22.
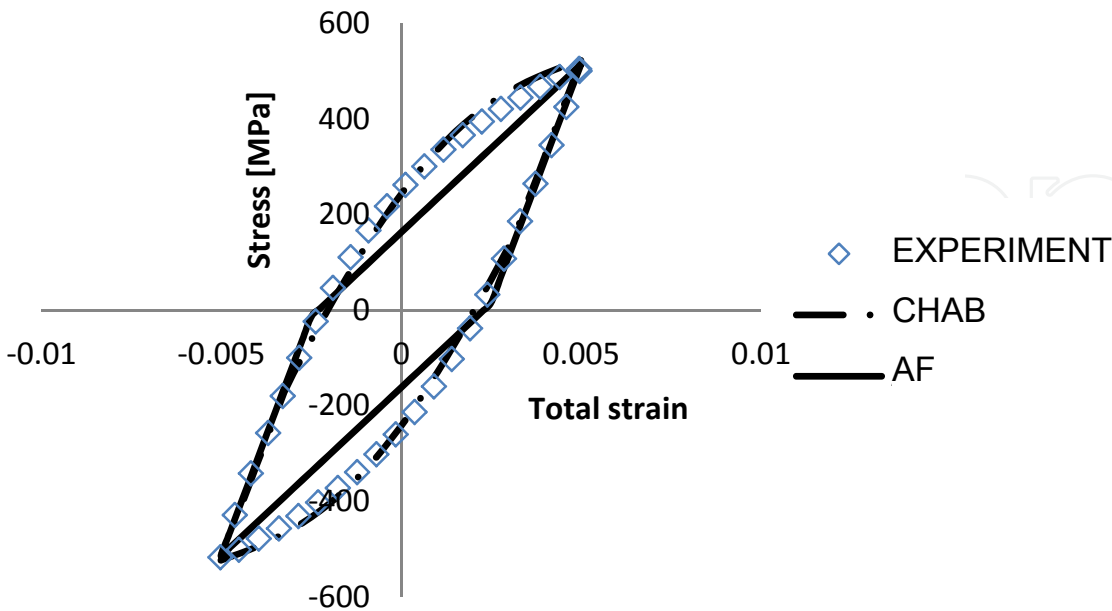

Fig. 21. Saturated uniaxial hysteresis loop and its prediction by AF and CHAB models.
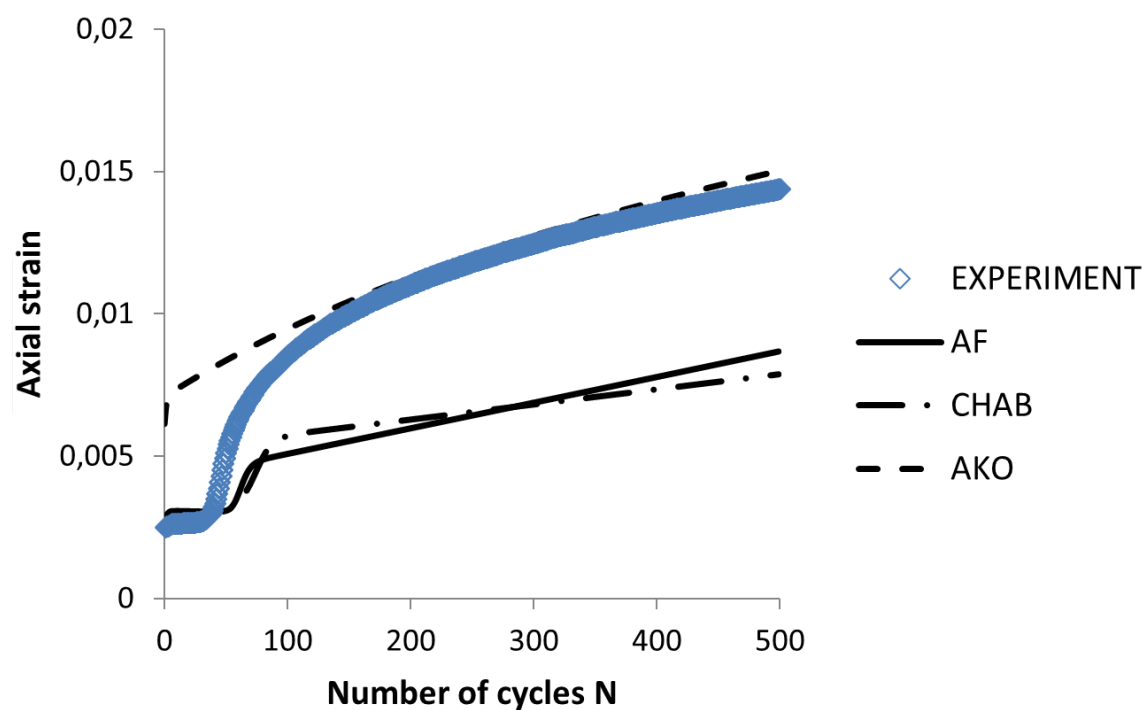
Fig. 22. Comparison of uniaxial ratcheting predictions with experiment (case D).

The results of multiaxial ratcheting predictions corresponding to simulations of the low cycle fatigue test performed under tension/torsion non-proportional (case A: 150 cycles with σ_a = 125MPa and τ_a = 300MPa) and proportional loading (case C: 100 cycles with σ_a = 225MPa and τ_a = 65MPa) are displayed in Fig. 23.
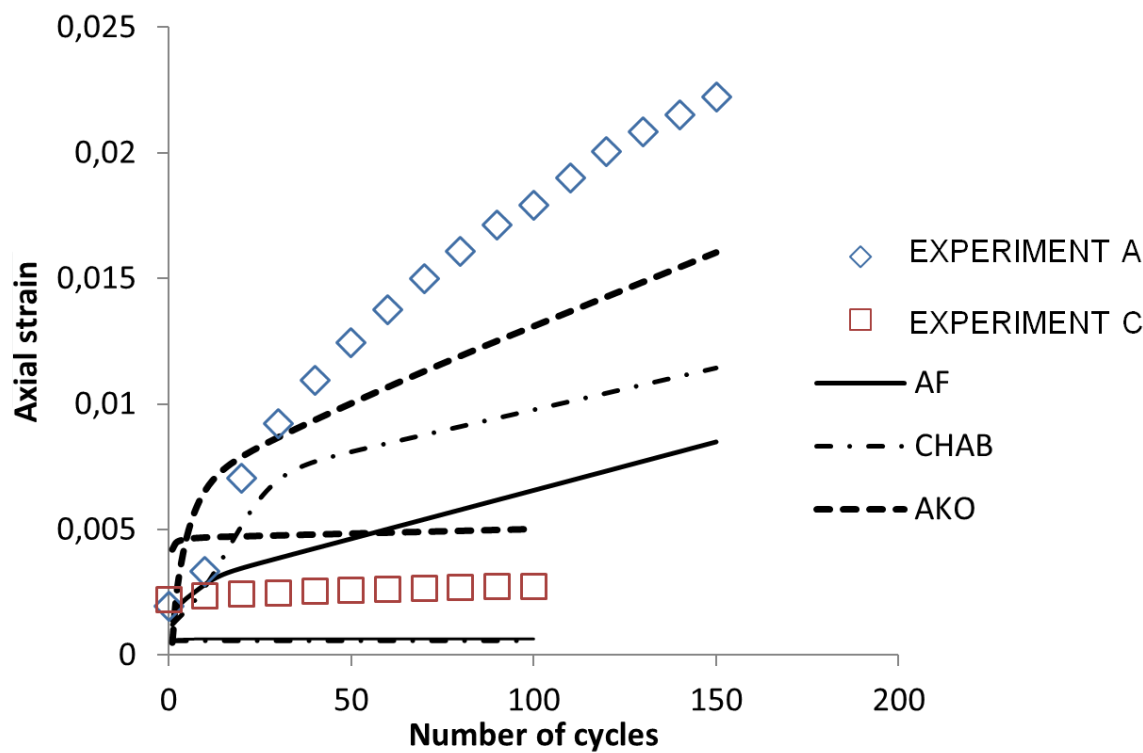

Fig. 23. Comparison of multiaxial ratcheting predictions with experiment (cases A and C).

The models CHAB and AF contain the nonlinear isotropic hardening rule (39), which enables to describe cyclic softening in initial cycles, see Fig.22. On the other hand, ratcheting prediction is better in the case of AbdelKarim-Ohno model. The same conclusion we have for simulations of the last loading case (case B: 500 cycles with $\sigma_a = 490MPa$ and $\tau_a = 170MPa$, 250 cycles with $\sigma_a = 490MPa$ and $\tau_a = 115MPa$, 250 cycles with $\sigma_a = 490MPa$ and $\tau_a = 215MPa$) as can be seen at the Fig. 24.
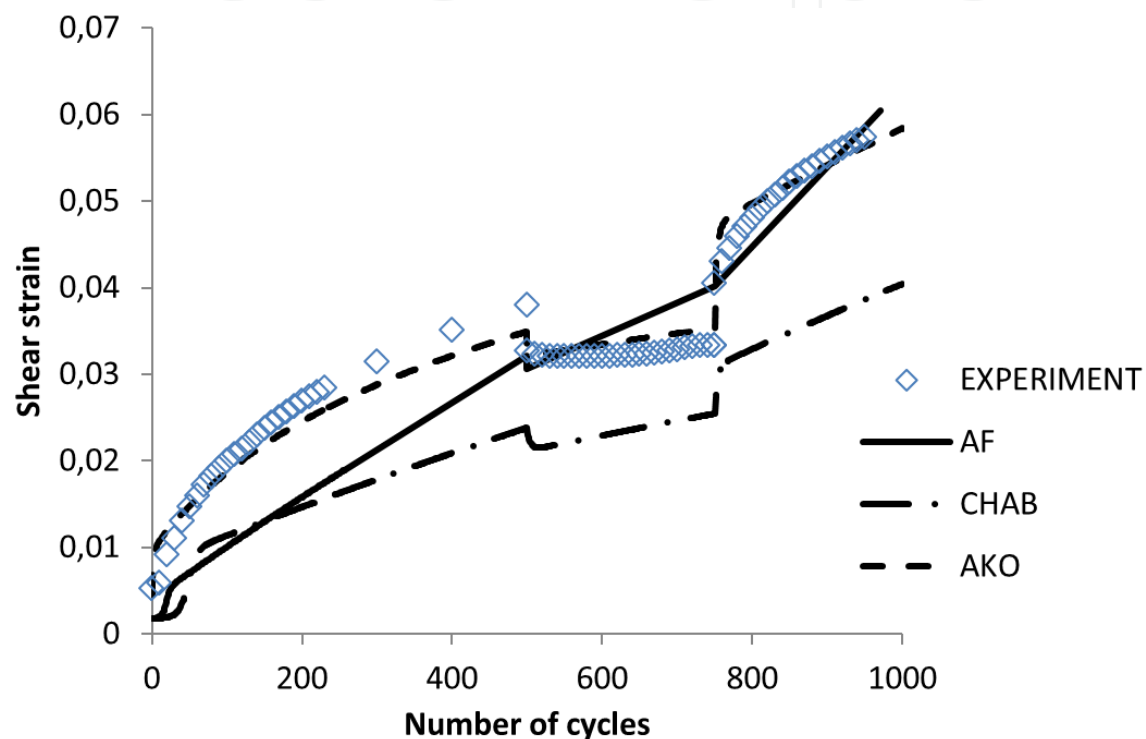
Fig. 24. Comparison of multiaxial ratcheting predictions with experiment (case B).

5. Conclusion

Background of the particular effects in cyclic plasticity of metals explained in the second section makes possible to understand well described incremental theory of plasticity and main features of cyclic plasticity models of Chaboche type. There have been shown interesting results of fatigue test simulations with emphasis on cyclic creep (ratcheting) prediction. It can be concluded from the results of simulations of the section 4 that used combined hardening model of Chaboche with two backstress parts can fairly well predicts the trend of accumulation of plastic deformation (ratcheting) for uniaxial and multiaxial loading cases, even under non-proportional loading, in comparison with the experimental observations of the R7T wheel steel. Indeed, the AbdelKarim-Ohno model gives better prediction of ratcheting for all cases than Armstrong-Frederick and Chaboche model.

6. Acknowledgment

7. References

Abdel-Karim, M. & Ohno, N. (2000). Kinematic Hardening Model Suitable for Ratchetting with Steady-State, *International Journal of Plasticity* 16, p. 225-240.

Armstrong, P.J. & Frederick, C.O. (1966). A Mathematical Representation of the Multiaxial Bauschinger Effect, *G.E.G.B. Report RD/B/N*, 731.

Bari, S. & Hassan, T. (2000). Anatomy of Coupled Constitutive Models for Ratcheting Simulations. *International Journal of Plasticity* 16, p. 381-409.

Bari, S. & Hassan, T. (2001). Kinematic Hardening Rules in Uncoupled Modeling for Multiaxial Ratcheting Simulation. *International Journal of Plasticity* 17, p. 885-905.

Burlet, H. & Cailletaud, G. (1987). Modelling of cyclic plasticity in Finite element codes. In: Proc. of 2nd Conference on Constitutive Laws for Engineering Materials: Theory and Applications, Elsevier, New York, p. 1157-1164.

Besseling, J.F. (1958). A Theory of Elastic, Plastic, and Creep Deformations of an Initially Isotropic Material Showing Anisotropic Strain-Hardening, Creep Recovery, and Secondary Creep. *Journal of Applied Mechanics*, vol. 25, p. 529-536.

Chaboche, J. L. & Lemaitre, J. (1990). *Mechanics of Solid Materials.* Cambridge University Press, Cambridge, ISBN 0-521-47758-1

Chaboche, J.L. & Dang Van, K. & Cordier, G. (1979). Modelization of The Strain Memory Effect on The Cyclic Hardening of 316 Stainless Steel, In: *5th International Conference on Structural Mechanics in Reactor Technology, Division L11/3*, Berlin, 13.-17. August 1979, Ed. Jaeger A and Boley B A. Berlin: Bundesanstalt für Material prüfung, p.1-10.

Chaboche, J. L. & Nouailhas, D. (1989). *Constitutive Modeling of Ratchetting Effects -Part I: Experimental Facts and Properties of the Classical Models*, Journal of Engineering Materials and Technology, Vol. 111, p. 384-416.

Chaboche, J.L. (1991). On some modifications of kinematic hardening to improve the description of ratcheting effects. *International Journal of Plasticity* 7, p. 661-678.

Chaboche, J.L. (1994). Modelling of ratchetting: evaluation of various approaches. *European Journal of Mechanics, A/Solids* 13, p. 501-518.

Chen, X. & Jiao, R. (2004). Modified kinematic hardening rule for multiaxial ratchetting prediction. *International Journal of Plasticity* 20, p. 871–98.

Chen, X. & Jiao, R. & Kim, K.S. (2005). On the Ohno-Wang Kinematic Hardening Rules for Multiaxial Ratchetting Modeling of Medium Carbon Steel, *International Journal of Plasticity* 21, p. 161–184.

Dafalias, Z.F. & Popov, E.P. (1976). Plastic Internal Variables Formalism of Cyclic Plasticity, *Journal of Applied Mechanics* 43, p. 645–650.

Doquet, V. & Clavel, M. (1996). Stacking-fault energy and cyclic hardening of FCC solid solutions under multiaxial non-proportional loadings. In: Pineau, A., Cailletaud, G., Lindley, T.C. (Eds.), *Multiaxial Fatigue and Design*, ESIS 21. Mechanical Engineering Publication, London, pp. 43–60.

Döring, R. & Hoffmeyer, J. & Seeger, T. & Vormwald M. (2003). A plasticity model for calculating stress–strain sequences under multiaxial nonproportional cyclic loading. Computl Mater Sci, 2003, Vol. 28, p. 587–96.

Halama, R. (2008). A Modification of AbdelKarim-Ohno Model for Ratcheting Simulations. *Technical Gazette* 15 (3), p. 3-9. ISSN 1330-3651

Halama, R. & Fojtík, F. & Brumek, J. & Fusek, M. (2009). Ratcheting measurement during fatigue testing. In: *Proceedings of the 11th International Conference Applied Mechanics 2009*, April 6–8, Slovakia, pp. 43–44.

Jiang, S. & Sehitoglu, H. (1996). Modeling of Cyclic Ratchetting Plasticity, Part I: Development of Constitutive Relations, Part II: Comparison of Model Simulations With Experiment. *Journal of Applied Mechanics* 63, p. 720-733.

Jiang, Y. & Zhang, J. (2008). Benchmark experiments and characteristic cyclic plastic deformation behavior. *International Journal of Plasticity*, 2008, Vol. 24, p. 1481–1515.

Kang, G.Z. & Gao, Q. & Yang, X.J. (2004). Uniaxial and multiaxial ratcheting of SS304 stainless steel at room temperature: experiments and viscoplastic constitutive model. *Int J Non-linear Mech* 39, p. 843–57.

Kurtyka, T. (1988). Parameter identification of a distortional model of subsequent yield surfaces. *Arch. Mech.* 40 (4), p. 433-454.

McDowell, D.L. (1995). Stress state dependence of cyclic ratchetting behavior of two rail steels, *International Journal of Plasticity* 11 (4) 397–421.

Mroz, Z. (1967). On the Description of Anisotropic Work-Hardening, *Journal of the Mechanics and Physics of Solids* 15, p. 163–175.

Ottosen, N.S. & Ristinmaa, M. (2005). *The Mechanics of Constitutive Modeling.* Elsevier Ltd. Sweden. ISBN 978-0-08-044606-6

Ohno, N. & Wang, J.D. (1993). Kinematic Hardening Rules with Critical State of Dynamic Recovery, Part I: Formulation and Basic Features for Ratchetting Behavior, *International Journal of Plasticity* 9, p. 375-390.

Prager, W. (1956). A New Method of Analysing Stresses and Strains in Work Hardening Plastic Solids. *Journal of Applied Mechanics* 23, p. 493-496.

Valanis, K. C. (1971) A theory of viscoplasticity without a yield surface. Part I: General theory. *Arch. Of Mechs.* 23, p. 217.

Vincent, L. & Calloch, S. & Marquis, D. (2004). A general cyclic plasticity model taking intoaccount yield surface distortion for multiaxial ratchetting. *International Journal of Plasticity* 20, p.1817–1850.

Williams, J.F. & Svensson, N. L. (1971). Effect of torsional prestrain on the yield locus of 1100-F aluminium. *Journal of Strain Analysis*, Vol. 6, p. 263.

Yaguchi, M. & Takahashi, Y. (2005). Ratcheting of viscoplastic material with cyclic softening, part 2: Application of constitutive models. *International Journal of Plasticity* 21, p. 835–860.

Ziegler, H. (1959). A modification of Prager's hardening rule. *Quart. Appl. Math.* 17, p. 55-65.
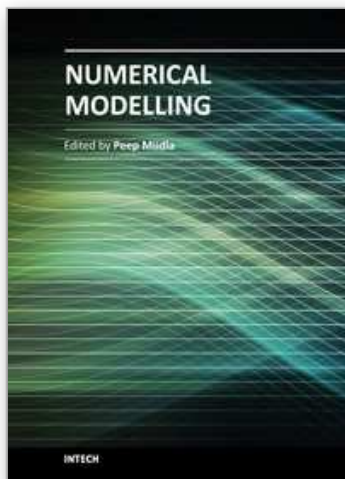
Numerical Modelling

Edited by Dr. Peep Miidla

This book demonstrates applications and case studies performed by experts for professionals and students in the field of technology, engineering, materials, decision making management and other industries in which mathematical modelling plays a role. Each chapter discusses an example and these are ranging from well-known standards to novelty applications. Models are developed and analysed in details, authors carefully consider the procedure for constructing a mathematical replacement of phenomenon under consideration. For most of the cases this leads to the partial differential equations, for the solution of which numerical methods are necessary to use. The term Model is mainly understood as an ensemble of equations which describe the variables and interrelations of a physical system or process. Developments in computer technology and related software have provided numerous tools of increasing power for specialists in mathematical modelling. One finds a variety of these used to obtain the numerical results of the book.

INTECH
open science | open minds